

Computing Complete Solution Sets for Approximate Four-bar Path Synthesis

Caroline Hills^a, Aravind Baskar^a, Mark Plecnik^a, Jonathan D. Hauenstein^a

^aUniversity of Notre Dame, Notre Dame, 46556, Indiana, USA

Abstract

The approximate path synthesis of four-bar linkages has been framed and solved with many different optimization techniques. Here we present a polynomial objective that is invariant to the number of approximate design positions selected, and a solution technique capable of finding all minima. The invariance property caps compute time despite increasing the size of input task specification data. This is performed by collecting a variable amount of task data into an invariable number of polynomial coefficients, called *moments*, before numerical optimization begins. The minima are found by applying the method of random monodromy loops to the zero gradient polynomial system of the aforementioned objective. This procedure finds all critical points, including the local and global minimum, and provides an in-process estimate of the percentage of critical points found. We applied our methodology to four-bar path synthesis problems of various computational scales by altering dimensional pre-specifications. The most general case was estimated to have $1,820,238 \pm 3810$ critical points, while pre-specification of one or two ground pivots yielded 26,052 and 503 roots, respectively, as validated by a trace test. The results are applied to a variety of examples.

Keywords: Kinematic synthesis, Optimization, Homotopy continuation

PACS: 0000, 1111

2000 MSC: 0000, 1111

1. Introduction

The approximate path synthesis of linkages is often formulated and solved as an optimization problem. Algorithms constructed from the current selection of optimization techniques can be used to find (1) one design option, (2) several stochastically generated design options, or (3) a Pareto front of design options. Apart from the choice of optimization technique, the choice in how to construct an objective(s) yields widely varying results. In this work, we aim to compute nearly *complete* solutions to approximate kinematic synthesis problems. That is, we form nonconvex polynomial objectives and then apply polynomial homotopy continuation to first-order conditions to compute critical points. Our work is primarily advantageous over past research in that it removes guesswork over the superiority of local minima, can find minima with small regions of attraction, and, since it aims to find all minima, we can cross-compare them over auxiliary considerations neglected by the objective.

In a sense, our approach is basic in that we outright compute all stationary points from first-order conditions. However, such computations have been prohibitive in the past due to the scale of the computation. The enabling technology is the new algorithms and advances in polynomial homotopy continuation [39], notably, the method of random monodromy loops [16, 11, 3, 4, 18]. Although computational power has increased dramatically over the past decades, without the algorithmic advances of homotopy continuation, there would be no route forward to solving the problems approached in this paper.

The problems solved in this paper are related to path synthesis for the four-bar linkage (schematically shown in Fig. 2). In such a problem, a planar path is prescribed for a point connected to the coupler link of a four-bar to trace. The goal is to compute the dimensions of a four-bar which can approximately reproduce this path. The scale of the computation required to *completely* solve such an optimization problem can be varied by installing simplifications in the form of pre-specified dimensions, which essentially reduce the dimension of the design space. In this vein, we form three different optimization problems: approximate path synthesis for a four-bar with (1) no dimensions pre-specified, (2) one ground pivot pre-specified, and (3) both ground pivots pre-specified. The first uses the most computational resources while the last requires the

least. For each of these problems, we conduct an *ab initio* computation to estimate the generic number of critical points each optimization problem has. This is performed by forming numerically general versions of the first-order conditions and solving them with the method of random monodromy loops. The size of these finite root sets are analyzed statistically to place confidence bounds on its accuracy [18] and, if possible, certified to be complete using a trace test [17, 8]. The resulting numerically generic finite root datasets can be applied as starting points with *parameter homotopies* [27] to solve for practical (not numerically generic) engineering design problems. Such parameter homotopies track fewer paths and thus use less computational resources. We demonstrate this functionality for a variety of examples in this paper.

Literature Review

If all dimensions of a four-bar are set to be design variables, then it can be shown that the four-bar can move a coupler point exactly through nine prescribed points generically. Wampler et al. [43] applied homotopy continuation to this problem and found the relevant polynomial system to generically have 8,652 finite roots which naturally has a 2-way symmetry from relabeling and a 3-way symmetry from Roberts’ cognates [32]. Hence, there are 1,442 distinct four-bar coupler curves that pass exactly through nine prescribed points generically thereby solving Alt’s problem [1]. If the two ground pivots of a four-bar are pre-specified and the rest of the dimensions are set to be design variables, then it can be shown that the four-bar can move a coupler point exactly through five prescribed points. Several authors [28, 41, 40] applied homotopy continuation to this problem and found the relevant polynomial system to generically have 36 nondegenerate, finite roots. In this work, we address analogous problems but applied to the approximate case, that is, N -point approximate synthesis.

By alleviating the exactness requirement on the coupler trace, approximate synthesis techniques allow for a greater number of prescribed task points. These formulations lead to nonlinear optimization problems with many local minima. Examples of nonlinear programming techniques that find only a single minima include [13, 22]. As a slight improvement, the initial guess of the nonlinear program could be varied systematically [7] or randomly [21] to hopefully discover more minima. Similar to this work, other authors [33] have considered working directly with the first-order necessary conditions, and Rao algorithms [31] explore the solution population through iterative updates to ultimately find the optimal solution.

Metaheuristic algorithms [37, 20, 26, 10, 12, 9, 34, 36] are less prone to settling on an inferior local minimum. Additionally, these algorithms need no derivative information, no initial guess (usually), and are capable of generating a Pareto front to accommodate multiple objectives. Combining heuristics in trajectory synthesis affords suitable and optimum solutions even in up to 14-bar linkage mechanisms [15].

However, metaheuristic algorithms are stochastic in nature, require hyper-parameter tuning, and do not necessarily guarantee one will find a global minimum or a complete view of the optimization landscape.

Approximate synthesis techniques accommodate the approximate nature of most practical design problems. Exact synthesis methods are often criticized as few practical design problems require such exactness. However, their appeal comes in the form of their deterministic nature and, assuming complete solutions are obtained, their ability to generate multiple design options of diverse forms. This paper aims to bring that aspect of completeness to approximate synthesis. Rather than using the approximate points directly in the formulation, our approach formulates an objective based off the moments of path points. Setting its gradient equal to zero leads to a square polynomial system in the design variables. Since this polynomial system is highly nonlinear, it possesses many roots, indicating the locations of critical points and potential minima. Polynomial homotopy continuation [6] is applied to a numerically general version of this system in order to characterize the size of its solution set and compute start points for later parameter homotopies. Statistical estimates [18] yield confidence bounds on the root count and, when possible, a trace test [17, 8] is applied to certify the root counts from the previous step. Our work up until this point is numeric but nonetheless generic and conclusive. Parameter homotopies are used to compute results for specific design problems.

In the proceeding, we formulate synthesis equations and describe our numerical methods in Section 2. Next, we approach three four-bar path synthesis problems with various simplifications installed. We consider approximate path synthesis when no dimensions are pre-specified (Section 3), when one ground pivot is pre-specified (Section 4), and when both ground pivots are pre-specified (Section 5). In each case, we present practical design scenarios to showcase the utility of our approach. Section 7 summarizes the contribution.

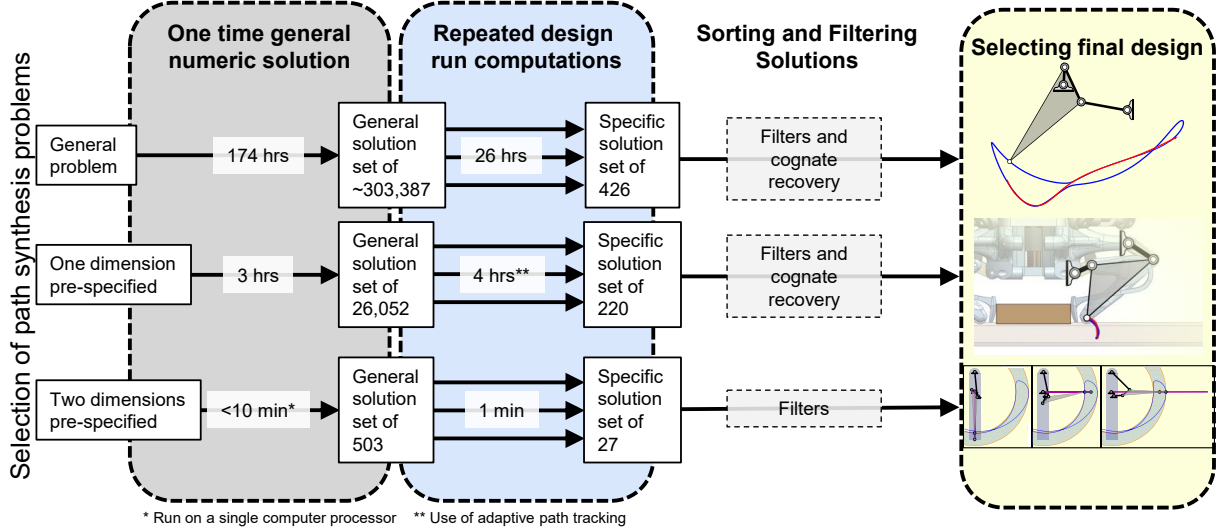


Figure 1: Graphical summary of the proposed method for solving the approximate path synthesis design problem.

2. Mathematical Formulation

2.1. Approximate Synthesis Equations

Consider the four-bar linkage shown in Fig. 2. Let A and B be the ground pivots of the linkage, and let l_1, l_2, l_3 be the moving link lengths as shown with angular displacements, measured counter-clockwise from the x -axis, as ϕ_1, ϕ_2, ϕ_3 , respectively. The coupler trace point is represented as P in the local frame of the coupler.

We introduce a vector variable Q such that

$$Q = \frac{P}{l_2},$$

which represents the vector P normalized by the coupler base, l_2 in the local frame. The coupler trace point in the global frame is denoted with the vector X . The use of isotropic coordinates with complex variable/parameter and its respective conjugate rather than Cartesian scalar coordinates afford simpler mathematical descriptions among other advantages.

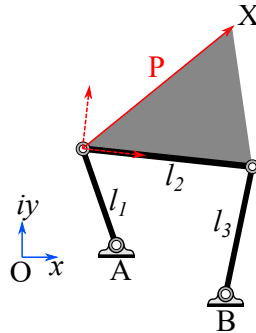


Figure 2: Schematic of a four-bar linkage for path synthesis.

However, one can always linearly transform between the two coordinate representations [42]. The transformation of real-valued Cartesian coordinates to isotropic is given by

$$z = x + yi, \quad \bar{z} = x - yi$$

Where x and y are real values and z is a complex value and \bar{z} is its conjugate. The transformation from isotropic to Cartesian is given by

$$x = \frac{z + \bar{z}}{2}, \quad y = \frac{z - \bar{z}}{2i}$$

Denote $\Phi_k = e^{i\phi_k}$ for $k = 1, 2, 3$ be the 2D rotation operators. Then, the vector loop equations for the left and right dyads are, respectively,

$$A + l_1\Phi_1 + l_2Q\Phi_2 = X, \quad (1a)$$

$$B + l_3\Phi_3 + l_2(Q - 1)\Phi_2 = X. \quad (1b)$$

Since we are working in isotropic coordinates, the conjugate relationship of the vector loops must be upheld. We denote conjugates with $*$ and note that the conjugate of a rotation operator is its reciprocal. That is, for a complex value $z = a + bi$, its conjugate is $z^* = a - bi$, and for a rotation operator θ , its conjugate is $\theta^* = \frac{1}{\theta}$. Additionally, since the link lengths are real-valued, they have no imaginary component and $l_k^* = l_k$ for $k = 1, 2, 3$. Hence, the conjugate loop equations are

$$A^* + l_1\frac{1}{\Phi_1} + l_2Q^*\frac{1}{\Phi_2} = X^*, \quad (2a)$$

$$B^* + l_3\frac{1}{\Phi_3} + l_2(Q^* - 1)\frac{1}{\Phi_2} = X^*. \quad (2b)$$

The rotation operators are not final design specifications, so they can be eliminated from the loop equations. Eliminating Φ_1 between Eq. 1a and Eq. 2a results in the equation

$$l_2Q^*(A - X) + (XX^* - A^*X - AX^* - l_{1s})\Phi_2 + l_2Q(A^* - X^*)\Phi_2^2 = 0, \quad (3)$$

where $l_{1s} = l_1^2 - l_2^2QQ^* - AA^*$. Likewise, we eliminate Φ_3 between Eq. 1b and Eq. 2b to obtain the second equation

$$l_2(Q^* - 1)(B - X) + (XX^* - B^*X - BX^* - l_{3s})\Phi_2 + l_2(Q - 1)(B^* - X^*)\Phi_2^2 = 0, \quad (4)$$

where $l_{3s} = l_3^2 - l_2^2(Q - 1)(Q^* - 1) - BB^*$.

To eliminate Φ_2 , we take note that the operator appears in both Eq. 3 and Eq. 4 quadratically and define a Sylvester's matrix representation using the previous two polynomials:

$$\eta(\mathbf{d}; X, X^*) = \begin{vmatrix} Q^*(A - X) & g(X, X^*) & l_2Q(A^* - X^*) & 0 \\ 0 & l_2Q^*(A - X) & g(X, X^*) & Q(A^* - X^*) \\ (Q^* - 1)(B - X) & h(X, X^*) & l_2(Q - 1)(B^* - X^*) & 0 \\ 0 & l_2(Q^* - 1)(B - X) & h(X, X^*) & (Q - 1)(B^* - X^*) \end{vmatrix} \quad (5)$$

where $g(X, X^*) = XX^* - A^*X - AX^* - l_{1s}$ and $h(X, X^*) = XX^* - B^*X - BX^* - l_{3s}$. Note that l_2 is a common nonzero factor to columns 1 and 4, therefore we drop it from the matrix expression. We capitalize on the further numerical advantages provided by substituting $l_{2s} = l_2^2$ in the expanded form of Eq. 5.

The determinant of the Sylvester's matrix eliminates Φ_2 and describes a polynomial representation of the coupler trace of a four-bar linkage with the variables $\mathbf{d} = \{A, A^*, B, B^*, l_{1s}, l_{2s}, l_{3s}, Q, Q^*\}$. This determinant is also known as a *tri-circular sextic curve* because, in addition to being real-valued, it is of degree six in (X, X^*) . Each X and X^* only appear with degree up to 3, implying a circularity of three [42].

This tri-circular sextic determinant condition is upheld for all four-bar linkages and their respective Roberts' cognates [32]. We denote this determinant condition as $\eta(\mathbf{d}; \mathbf{p}_j)$ where \mathbf{d} is the set of design variables as previously defined and $\mathbf{p}_j = (X_j, X_j^*)$ are the design parameters, the positions in space through which we intend our determinant curve to intersect. We intend to minimize the sum of squares of a function residual rather than the distance between specified and synthesized points. It is important to note there

are other ways to formulate an objective for approximate synthesis depending on the error one wishes to minimize [14].

From here on, we will denote the determinant curve with specified design positions as $\eta_j = \eta(\mathbf{d}; \mathbf{p}_j)$.

Consider the path generation problem for positions (X_j, X_j^*) for $j = 1, \dots, N$ where N is the number of positions. It is well known that Alt's problem [1] for $N = 9$ generic points is equivalent to solving the nine-dimensional square system $\eta_j = 0$ for $j = 1, \dots, 9$. When $N > 9$ and the design positions are generic, the exact path synthesis problem has no solutions; therefore, one must describe a formulation for an approximate path synthesis.

Our method of approximation minimizes the residuals of the coupler-trace equation previously described based on an L_2 -norm measure. This sum-of-squares measure preserves the system's polynomial nature and is real-valued. That is, one aims to solve the unconstrained optimization problem $\min \sum_{j=1}^N \eta_j^2$ by computing all solutions to the respective first-order optimality conditions:

$$\sum_{j=1}^N \eta_j \frac{\partial \eta_j}{\partial \mathbf{d}} = \mathbf{0}. \quad (6)$$

This problem can, and has been, solved at face value, by preserving the use of design positions as the system's parameters [2].

There theoretically is no limit to the specified number N of design positions in this formulation. However, using as many as up to $N = 20$ positions introduces additional parameter terms into already verbose expressions, thus increasing computational costs. Since these design positions appear nonlinearly in η_j , we propose an alternative parameterization that instead works with the essential information of the design positions.

The essential information is captured by the *moments* of the data. Recall that moments mathematically provide descriptive measurements of data. For example, the first moment of a probability distribution is the mean which describes the center of probability mass. By expanding the objective function in (6), and collecting coefficients on the sum of design positions, one observes that the determinant curve depends linearly upon 47 moments of the monomials of (X_j, X_j^*) for $j = 1, \dots, N$ that appear within the coupler equation. These moments are of the form

$$\frac{1}{N} \sum_{j=1}^N X_j^a X_j^{*b} \quad (7)$$

where $0 \leq a, b \leq 6$, because, recall that the coupler curve is tri-circular sextic, X, X^* can be at most degree six. In theory, there are $7 \cdot 7 = 49$ moments; however, $(a, b) = (0, 0)$ is a constant value of 1 and $(a, b) = (6, 6)$ does not appear in the expansion, so we retain $49 - 2 = 47$ moments.

Let $\mathbf{g} = \{g_1, g_2, \dots, g_{47}\}$ be the set of the moment parameters with

$$g_1 = \frac{1}{N} \sum_{j=1}^N X_j, \quad \dots, \quad g_{47} = \frac{1}{N} \sum_{j=1}^N X_j^6 X_j^{*5}.$$

Each moment in \mathbf{g} depends on the exponents (a, b) as in (7). For the general case with no pre-specified dimensions, the 47 moments correspond with the exponents (a, b) in Table 1. When one or both pivot locations are pre-specified, the 41 moments correspond with the exponents (a, b) in Table 2. Note that the lesser number of moments between the no pre-specified dimensions and one and two pre-specified dimensions cases is a consequence of defining a pivot location at the origin, which was assigned to pivot $B = B^* = (0, 0)^T$ without loss of generality.

In particular, the pre-specification of the B and B^* pivot location results in the original monomials corresponding to $g_5 = (0, 5), g_6 = (0, 6), g_{13} = (1, 6), g_{35} = (5, 0), g_{42} = (6, 0)$, and $g_{43} = (6, 1)$ vanishing in this new set of 41 moments.

With this new formulation, one have an equivalent representation of the objective function we denote as

$$\psi(\mathbf{d}; \mathbf{g}) = \sum_{j=1}^N \eta(\mathbf{d}; \mathbf{p}_j) \quad (8)$$

1 = (0,1)	7 = (1,0)	13 = (1,6)	19 = (2,5)	25 = (3,4)	31 = (4,3)	37 = (5,2)	43 = (6,1)
2 = (0,2)	8 = (1,1)	14 = (2,0)	20 = (2,6)	26 = (3,5)	32 = (4,4)	38 = (5,3)	44 = (6,2)
3 = (0,3)	9 = (1,2)	15 = (2,1)	21 = (3,0)	27 = (3,6)	33 = (4,5)	39 = (5,4)	45 = (6,3)
4 = (0,4)	10 = (1,3)	16 = (2,2)	22 = (3,1)	28 = (4,0)	34 = (4,6)	40 = (5,5)	46 = (6,4)
5 = (0,5)	11 = (1,4)	17 = (2,3)	23 = (3,2)	29 = (4,1)	35 = (5,0)	41 = (5,6)	47 = (6,5)
6 = (0,6)	12 = (1,5)	18 = (2,4)	24 = (3,3)	30 = (4,2)	36 = (5,1)	42 = (6,0)	

Table 1: Exponents (a, b) for the 47 moments in the general case

1 = (0,1)	7 = (1,2)	13 = (2,2)	19 = (3,1)	25 = (4,0)	31 = (4,6)	37 = (5,6)
2 = (0,2)	8 = (1,3)	14 = (2,3)	20 = (3,2)	26 = (4,1)	32 = (5,1)	38 = (6,2)
3 = (0,3)	9 = (1,4)	15 = (2,4)	21 = (3,3)	27 = (4,2)	33 = (5,2)	39 = (6,3)
4 = (0,4)	10 = (1,5)	16 = (2,5)	22 = (3,4)	28 = (4,3)	34 = (5,3)	40 = (6,4)
5 = (1,0)	11 = (2,0)	17 = (2,6)	23 = (3,5)	29 = (4,4)	35 = (5,4)	41 = (6,5)
6 = (1,1)	12 = (2,1)	18 = (3,0)	24 = (3,6)	30 = (4,5)	36 = (5,5)	

Table 2: Exponents (a, b) for the 41 moments when one or both ground pivots are pre-specified

which is linear in \mathbf{g} . The first-order optimality conditions yield $\nabla_{\mathbf{d}}\psi(\mathbf{d}; \mathbf{g}) = \mathbf{0}$, which are also linear in \mathbf{g} .

When moving to a different representation, it is a natural question to consider the image of the map between the two spaces. Namely, if the number of solutions is preserved between spaces. This can be addressed using [19, Lemma 3] which yields the following.

Proposition 1. *The image of the map from the design positions to the 47-dimensional moment space is full dimensional for sufficiently large N . In fact, this is guaranteed when $2N > 47$.*

The image from design positions to the moment space is dense. Hence, a sufficient condition for the generic number of roots using the moment-formulation and the design position-formulation agree when $2N > 47$.

However, it is not a necessary condition. One only needs to ensure $N > 9$ for optimal synthesis, but heuristically a lesser N will still admit an equivalent number of solutions between formulations.

Furthermore, by using a moment formulation, one can consider moments defined by discrete design position points or continuous families of design positions. For example, for a family $(X(s), X^*(s))$ with $s_0 \leq s \leq s_1$, one can replace (7) with

$$\frac{\int_{s_0}^{s_1} X(s)^a X^*(s)^b ds}{\int_{s_0}^{s_1} ds}. \quad (9)$$

Finally, although the moment parameters bear little physical meaning, their linear appearance improves both the local conditioning of the system and the solving of the system via random monodromy loops.

2.2. Random Monodromy Loops

A random monodromy loop (RML) is a numerical continuation technique that starts with an initial seed set of solutions given defined parameters, applies monodromy action, and ends the loop at the original set of parameters. In our RML method, the solution paths travel to pre-defined intermediary yet generic systems. The solution paths are not guaranteed to return to the original solution from which their path had started, so consequently the set of solutions the RML ends with can consist of both previously known solutions and new, valid solutions. Through iterative applications of RML and compilation of unique starting solutions, one efficiently computes the the system solutions.

First, we fixed a randomly selected set of moment parameters \mathbf{g}_s and obtained the respective variable solutions such that $\psi(\mathbf{d}; \mathbf{g}_s) = 0$. Since we are aiming to solve for the generic solution set of our system, this seed solution does not need to satisfy the conjugate relationship. Additionally, such a seed solution can be obtained using a local method such as Newton’s method or a Newton homotopy. With this seed, we employed RML along a triangular “loop” in the parameter space with our starting system at the vertex defined by the parameter set \mathbf{g}_s and the other two vertices defined by two intermediary generic system parameters, $\mathbf{g}_1, \mathbf{g}_2$, respectively. Since the parameters are linear, and a triangle is topologically equivalent to a circle, our RML consists of three applications of a straight-line homotopy along the three vertices of the triangle.

$$\begin{aligned}
H_1(\mathbf{d}; t) &= \psi(\mathbf{d}; \mathbf{g}_s)t + \psi(\mathbf{d}; \mathbf{g}_1)(1 - t), & t \in [0, 1], \\
H_2(\mathbf{d}; t) &= \psi(\mathbf{d}; \mathbf{g}_1)t + \psi(\mathbf{d}; \mathbf{g}_2)(1 - t), & t \in [0, 1], \\
H_3(\mathbf{d}; t) &= \psi(\mathbf{d}; \mathbf{g}_2)t + \psi(\mathbf{d}; \mathbf{g}_s)(1 - t), & t \in [0, 1].
\end{aligned} \tag{10}$$

Thus we accumulated a solution set to our system as defined by the parameter set \mathbf{g}_s . Starting from one seed solution, perfect tracking would leave 2 solutions after completing the first loop, 4 solutions after the second, 8 solutions after the third, and so on. While this iterative action increases the number of paths tracked and leads to improved rate of solution set saturation, it comes at a computational cost as we double the number of paths we track each loop. We note that our formulation, $\psi(\mathbf{d}; \mathbf{g})$ and the corresponding solution paths are invariant under Roberts' cognates. So we apply a cognate check between loops to ensure we track only one member per cognate group as the respective Roberts' cognate designs can be recovered through known transformations applied in post-processing of the solutions. This provides great efficiency in computing solutions to larger systems.

2.3. Schnabel Estimator

Since the number of isolated solutions is finite, such a doubling process in the collection of solutions can not continue indefinitely. Thus, by comparing the number of new solutions obtained with the number of repeated solutions per RML, one can obtain statistical estimates on the total number of solutions using a probabilistic ‘‘catch and release’’ model [18]. One such model is the Schnabel model.

When applied to biological populations, the Schnabel model relies on data from previous marks and captures to yield an estimator on the total number of a wild specie's population. In this paper, the population of interest and unknown size is the number of solutions to the *ab initio* solve of our experiments. We used a window size of three; the Schnabel estimator of the total solution count is dependent on data from the current and two previous RML applications.

The expressions of the Schnabel estimator, β , and its variance over the moving window size three as well as the 95% confidence interval bounds, respectively, are

$$\begin{aligned}
\beta &= \frac{\sum_{k=1}^3 \#S^{(k)} \cdot \#E^{(k)}}{\sum_{k=1}^3 \#(S^{(k)} \cap E^{(k)})}, \\
\text{var}(\beta^{-1}) &= \frac{\sum_{k=1}^3 \#(S^{(k)} \cap E^{(k)})}{(\sum_{k=1}^3 \#S^{(k)} \cdot \#E^{(k)})^2}, \\
&\left((\beta^{-1} - 1.96\sqrt{\text{var}(\beta^{-1})})^{-1}, (\beta^{-1} + 1.96\sqrt{\text{var}(\beta^{-1})})^{-1} \right).
\end{aligned} \tag{11}$$

Where $\#S$ is the number of solutions with which we start one RML application, $\#E$ is the number of solutions with which we end the RML application, and $\#(S \cap E)$ is the number of ‘‘repeat’’ solutions that belong to both sets S and E .

2.4. Trace Test

Although the number of compiled solutions and the Schnabel estimate provide confidence on the total number of solutions, one may wish to verify that all solutions have indeed been found. This can be accomplished via a 2-homogeneous trace test [17]. The 2-homogeneity arises from the design variables \mathbf{d} and the moment parameters \mathbf{g} . With such a test, one needs to collect two solution sets. The first set is computed as described previously with the moment parameters fixed. In the second set, one selects a design variable to be a parameter and selects a moment parameter to be a variable, and repeats the solving process as above. By using these two solution sets, the 2-homogeneous trace test [17] can determine if the solution sets are complete or not.

For the computations in this paper, we employed the second derivative trace test from [8, § 2.3] to avoid tracking additional paths. In particular, this *local trace test* approach simply relies upon computing local Jacobian and Hessian information of ψ to perform the trace test.

The following three sections utilize the aforementioned techniques on three formulations: the general case with no pre-specified dimensions, pre-specification of one ground pivot, and pre-specification of both ground

pivots, respectively. Each problem was first solved in an *ab initio* run using random monodromy loops with the size of the solution set tested using either a statistical probabilistic model on the RML iterations or a trace test computation, or both. Finally, in each of these three formulations, we present a real-world example application. All computations were run using Bertini[5] in parallel mode on a four node dual 192 core machine at the University of Notre Dame’s Center for Research Computing.

3. The General Case (No Pre-specification of Dimensions)

3.1. Ab Initio Computation

Following Section 2, the general case has design variables $\mathbf{d} = \{A, A^*, B, B^*, l_{1s}, l_{2s}, l_{3s}, Q, Q^*\}$ and moment parameters $\mathbf{g} = \{g_1, \dots, g_{47}\}$ as listed in C.5. With Roberts’ cognates and relabeling, the solutions arise in groups of 6 with formulas listed in Appendix A. With this setup, the RML procedure was used to determine the generic root count. Figure 3 shows the ratio of repeated solutions for the iterations and the Schnabel estimates with the 95% confidence interval based on groups of solutions, i.e., one-sixth of the total number.

We note that to further improve the conditioning of the system when performing the random monodromy loops, we redefined the grouping of the system’s variables for the homotopy. Additionally, for paths that failed between intermediary systems, we applied cognate transformations and reran the homotopy on those paths until we achieved a 100% path success rate or we exhausted each of the cognate transforms. This resulted in improving path success rate of approximately 95-97% per iteration. However, this came at an increase in the computational cost with the total time taking approximately 174 hours (7.25 days) for the *ab initio* solve.

Figure 3 shows 26 iterations of RML for the moment-parameterized system. The final count of distinct solution groups after the 26 RML iterations was 303,387 yielding $6 \cdot 303,387 = 1,820,322$ solutions in total. One can see in Fig. 3a that the initial RML iterations find almost exclusively new points while later iterations find almost no new points. For example, iterations 23-26 only produced 87 new solutions, hence there is strong confidence we have found $\sim 99.8\%$ of the solution set.

3.2. Solution Set Validation

From Fig. 3b, one observes that the 95% confidence interval shrinks quickly for the Schnabel estimate with a moving window of size 3 as the number of iterations increases. In particular, at iteration 26, the 95% confidence interval for the Schnabel estimate is $6 \cdot (303,373 \pm 635) = 1,820,238 \pm 3,810$ solutions. This is within a rather tight bound when regarding the size of the system, and the RML computation count from the previous section lies within this bound. The total isolated solution count is estimated to be upwards of

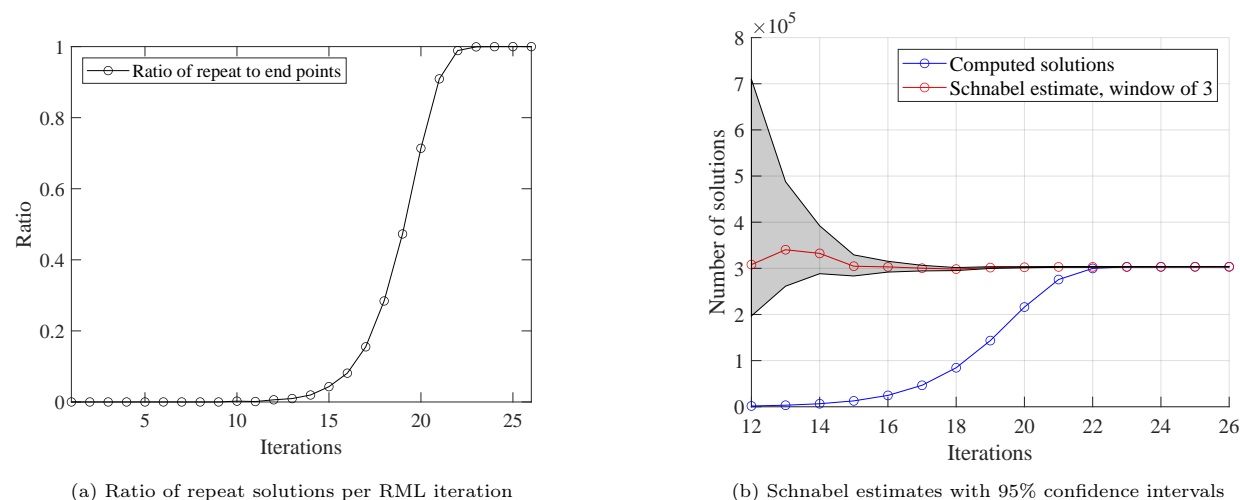


Figure 3: Computational summary of the *ab initio* solving for the general case formulation.

approximately two million solutions, cognate transformations included [2].

We did not employ a trace test on this system for two reasons. First, the set of known solutions is probably not complete and thus more iterations would be needed. Also, solving for the switched variable-parameter systems poses an equally arduous challenge. Therefore, for this problem, we rely upon the statistical estimates to provide that the solution set is nearly complete.

3.3. Applied Example

As an illustration of using this *ab initio* computation to solve an applied problem, we consider approximately replicating the curve in [35, Fig. 6]. This curve is traced by a Stephenson III six-bar mechanism with a torsion spring link. The mechanism is a locomotive hopping machine with three main trajectory phases: stance phase without spring activation, stance phase with spring activation, and swing phase.

The mechanism consists of three ground pivots, A, B, O , where the remaining pivot locations, C, D, E, F, P are described by the leg lengths $OC, AD, CE, DE, EF, BF, EP$, and FP . The torsion spring has an additional link OS , but, for simplicity, we assumed the torsion spring leg, described by the parameter OC , to be a constant length. The triangle formed between the pivots $OCAD$ that describes the location of pivot E has an internal angle of $\kappa_1 = -59.46^\circ$ and the triangle formed between the links $OCFB$ that describes the location of the coupler point P has an internal angle of $\kappa_2 = -18.63^\circ$.

The six-bar mechanism and coupler curve from which we extracted design positions to compute the 47 continuous moment parameters is shown in Fig. 4.

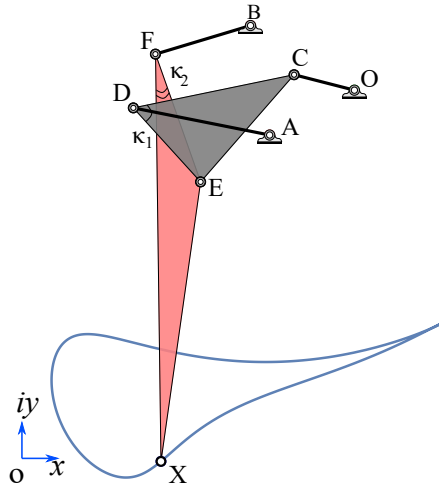


Figure 4: The six-bar mechanism and coupler curve used for the applied example of the general case.

Using the following parameters for the mechanism, we computed the 6-bar kinematics and obtained the coupler curve from [35, Fig. 6]. Note the pivot O is at the origin, so $O = O^* = 0 + 0i$.

$$\begin{aligned} A &= -3.81 - 2.02i, & A^* &= -3.81 + 2.02i, \\ B &= -4.67 + 2.91i, & B^* &= -4.67 - 2.91i \\ |OC| &= 2.8, & |AD| &= 6.25, & |CE| &= 6.40, & |DE| &= 4.50 \\ |EF| &= 6.10, & |BF| &= 4.46, & |EP| &= 12.71, & |FP| &= 18.34 \end{aligned}$$

We then extracted over a hundred sample points from the computed curve that belonged to the stance phases with and without spring activation as well as a subset of the swing phase to mimic the lift-off trajectory of the mechanism foot's from the ground. We re-parameterized the sample points to be equally spaced, rescaled them to the unit plane, generated an interpolating function, and used numerical integration to compute the continuous form of the 47 moment parameters needed for our parameter homotopy, as defined by Eq. 9. The numerical values of the continuous moments are given in Table C.5 in Appendix C.

The parameter homotopy tracked 303,387 paths from the generic parameters of the *ab initio* solve to the physically meaningful system. Using only double precision path tracking in about 26 hours of computational

time, 108,008 successfully tracked to nonsingular solutions. Of these, 71 corresponded to physically meaningful designs. Due to cognate transformations, listed in Appendix A, we computed the cognates of the 71 unique solutions and filtered for duplicate designs. As there were no duplicates, this resulted in a total of $6 \cdot 71 = 426$ potential physically meaningful solutions. Of the 71 distinct solutions, 2 are local minima and 69 are saddle points.

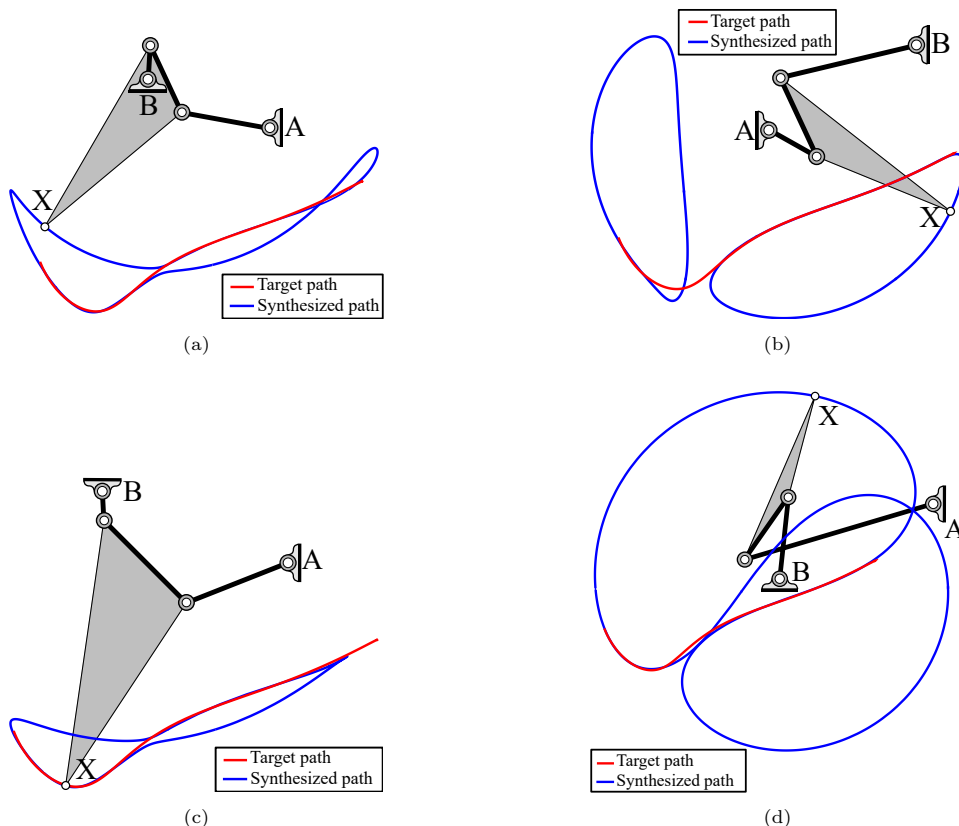


Figure 5: Example solutions of applied problem for the general case formulation that exhibit branch and circuit defective behavior.

Of the physically meaningful coupler curves, many had sections of their coupler curve that traced the design positions extremely well. However, these solutions faced either the issue of branch defects in the curve based on which pivot was actuated or impractical cognate design dimensions. One can see such cognate designs in Figs. 5. The synthesized coupler curve is shown in blue. Note that different actuation on pivots can result in branch defects on the coupler curve. Therefore, we present visualizations of only the curve and a cognate group member solution.

Table 3 gives the dimensions of the solutions presented in Fig. 5 as well as two error metrics - the value of the cost function and the maximum Euclidean distance, or maximum deviation (Max Dev in solution tables), between target points and their respective nearest point on the synthesized path. This example and the results suggest that the general case formulation is not computationally effective and one would benefit from working with a smaller problem, such as the system resulting from the designation of specifications on one or both ground pivots on the four-bar final design.

4. Pre-specification of One Ground Pivot

4.1. *Ab Initio* Computation

Consider the approximate synthesis problem obtained by specifying the ground pivot $B = B^* = 0$ with design variables $\mathbf{d} = \{A, A^*, l_{1s}, l_{2s}, l_{3s}, Q, Q^*\}$. Due to the designation of the one ground pivot at the origin, some moments have a zero coefficient and thus disappear within the computation. Thus, with this

	Fig 5a	Fig 5b	Fig 5c	Fig 5d
A	$-0.04055-0.3039i$	$-0.2168-0.3701i$	$0.3065-0.2725i$	$-0.01113-0.2719i$
A^*	$-0.04056+0.3039i$	$-0.2168+0.3701i$	$0.3065+0.2725i$	$-0.01113+0.2719i$
B	$-0.2985-0.1947i$	$0.08195-0.1943i$	$-0.08198-0.4600i$	$-0.3620-0.1379i$
B^*	$-0.2985+0.1947i$	$0.08195+0.1943i$	$-0.08198+0.4600i$	$-0.3620+0.1379i$
l_1	0.1897	0.1102	0.5006	0.2054
l_2	0.1594	0.1802	0.1981	0.2222
l_3	0.06938	0.2866	0.2086	0.05237
Q	$-0.6140+2.3195i$	$-1.2155-1.1248i$	$2.2589+0.4626i$	$-0.3771+1.8417i$
Q^*	$-0.6142-2.3195i$	$-1.2155+1.1248i$	$2.2589-0.4626i$	$-0.3771-1.8417i$
Cost	$4.9846 \cdot 10^{-8}$	$2.008746 \cdot 10^{-8}$	$2.8040 \cdot 10^{-7}$	$7.3460 \cdot 10^{-8}$
Max Dev	0.1149	0.2075	0.1813	0.09704

Table 3: Table of Fig 5 solutions and their dimensions and error metrics.

pre-specification, the system admits 41 moment parameters which are provided in in Table 2. Note that Proposition 1 still holds when $2N > 41$ for this reduced list of moments.

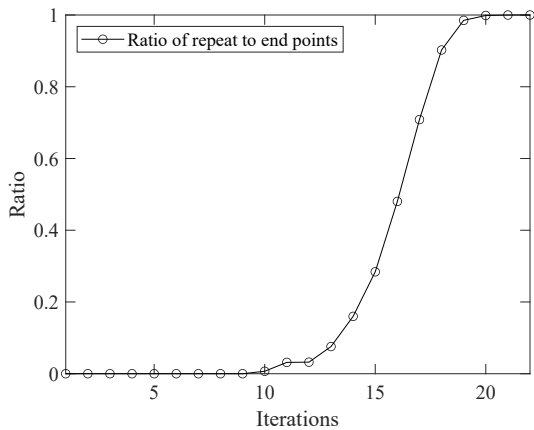
Using the RML procedure as previously described, the system reached convergence in 22 iterations to a final total solution count of 26,052 solutions as shown in Fig. 6 with a computation time of approximately 8.5 hours. The long computation time is attributed to the lack of stopping criteria on the RML code. The RML terminated after a set number of 30 iterations to ensure the total solution set was computed. Hence, there are superfluous iterations that were not essential to recovering the solution set. Had a different termination criteria be utilized, the computation time would be much faster.

Due to the specification of one ground pivot, solutions to this system come in cognate member groups of size 2 for 13,026 distinct solution groups with formulas listed in Appendix B. When using this cognate reduction to only track one path in each group as a check on our RML procedure and resulted in the same number of solutions, $2 \cdot 13,026 = 26,052$, that took approximately 100 minutes to compute.

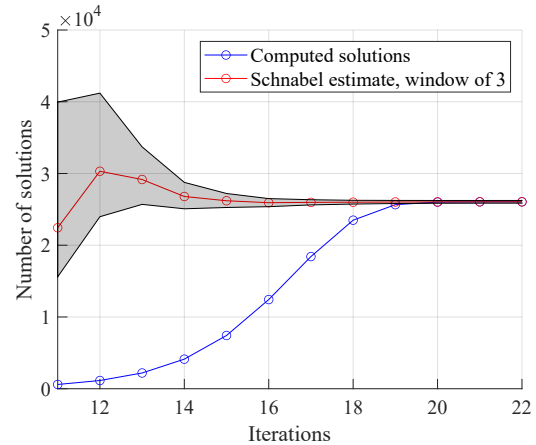
4.2. Solution Set Validation

As observed in Fig. 6b, the Schnabel estimates with a moving window of size 3 quickly tighten with the estimate after the 23rd iteration being $26,052 \pm 193$ solutions. With the tight Schnabel confidence interval and multiple runs that admitted the same number of solutions, this prompted using a trace test validation.

To utilize the 2-homogeneous trace test as summarized in Section 2.4, one needs to perform another solve where we switched the variable-parameter pair l_{1s} and g_1 . The resulting system produced 14,792 solutions and the 2-homogeneous trace test was then successfully applied to a total of $26,052+14,792 =$



(a) Ratio of repeat solutions per RML iteration



(b) Schnabel estimates with 95% confidence intervals

Figure 6: Computational summary of the *ab initio* solving when one ground pivot is pre-specified.

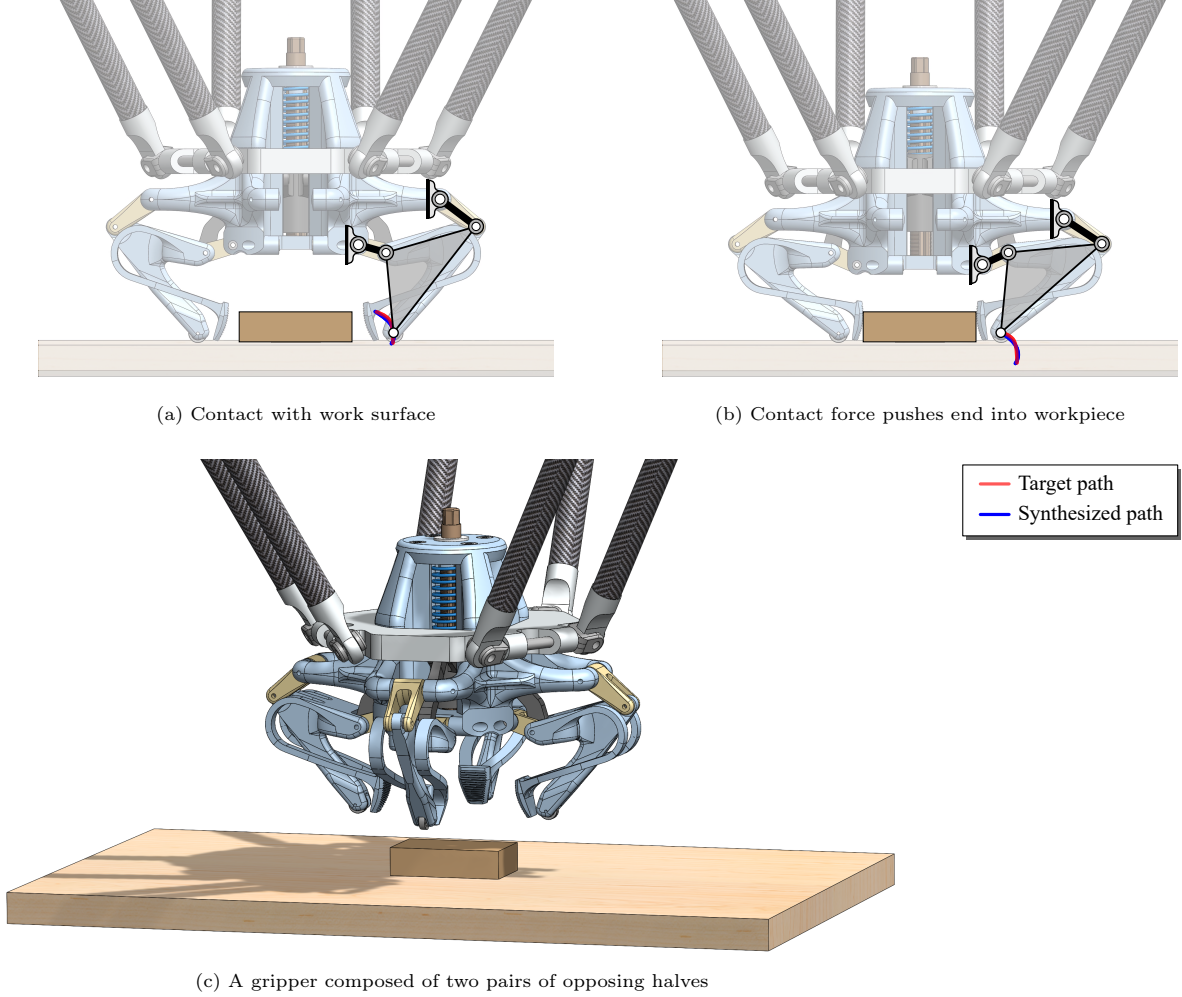


Figure 7: A candidate design from the pre-specification of one ground pivot computation. (a) After making contact with the work surface, (b) said surface pushes the gripper end up, relative to itself, and into a workpiece to be gripped. Contact with the work surface actuates the gripper, and the four-bar linkage guides its end into the workpiece. (c) Such a gripper might comprise of two pairs of opposing halves.

40,844 solutions. Thus, this trace test confirmation shows that 26,052 is indeed the precise solution count.

4.3. Applied Example

This system was applied to a gripping mechanism inspired by the solution present in [30, Fig. 5]. The original positions were chosen from [30] and fitted to a polynomial interpolation in order to define additional points for a total of $N = 20$ positions. The original pivot locations of the applied example are

$$A = -3.0432 + 4.5214i, \quad B = -0.5609 + 3.1702i$$

The other two joint dimensions are $C = 0.8155 + 2.008853i$ and $D = 1.09927 + 1.6694i$. To align this solution design with our pivot specification that $B = B^* = 0$, the B pivot of [30] was translated to the origin, and each real design position, including the additional interpolated points, was shifted by a difference of $-0.56 - 3.17i$ for B and $-0.56 + 3.17i$ for B^* . The shifted points were then divided by 3 so that their moments were within approximately unit magnitude. The shifted design positions are provided in Appendix C. After computing the corresponding moments, a parameter homotopy tracked 26,052 solutions in adaptive precision to the new system. The total computation time for this parameter homotopy was approximately four hours and resulted in the successful path tracking to 25,540 nonsingular solutions. Of those nonsingular solutions, 216 obeyed the physically meaningful complex-conjugate condition. Recall that in addition to these real solutions, their

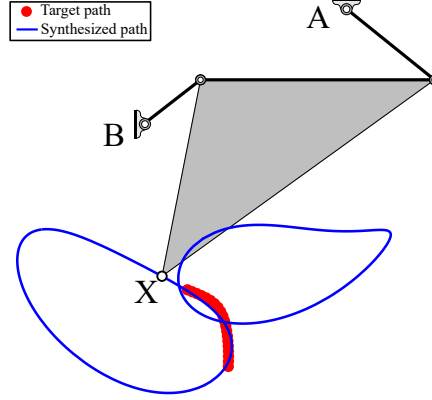


Figure 8: The solution design exhibiting preferred design characteristics for the one dimension pre-specified example.

respective cognates are also solutions. Since the B and B^* pivots are fixed at the origin, the valid cognate transformations must obey this pivot specification with formulas presented in Appendix B. We computed the cognates of these solutions, filtered for repeats, and filtered to retain one member per cognate group. This resulted in a total of 110 distinct coupler curves corresponding to physically meaningful solutions, or $2 \cdot 110 = 220$ total solution designs. Within these 110 distinct solutions, 20 are classified as minima and 90 are saddle points.

One such solution design and its respective synthesized path is presented in Fig. 8, the prototype mechanism based on that design is presented in Fig. 7a and Fig. 7b. A model of the prototype of the gripping mechanism using legs with the selected four-bar design to pick up a small block is shown in Fig. 7c.

The solution dimensions for this chosen design are given in Table 4. Note that this design is an saddle

A	$0.8773 + 0.4991i$
A^*	$0.8773 - 0.4991i$
B	0
B^*	0
l_1	0.4931
l_2	1.01719
l_3	0.3090
Q	$1.1648 + 0.8395i$
Q^*	$1.1648 - 0.8395i$
Cost	12.6198
Max Dev	0.1322

Table 4: Numerical values of the final chosen design solution for the one dimension pre-specified applied example.

point, and this solution was chosen qualitatively through a visual inspection of the solutions. The coupler solution and mechanism dimensions exhibited potential use that was not seen in solutions pertaining to the lowest objective costs. For reference, the ten solutions with the lowest costs are provided in Table D.9 in Appendix D.

5. Pre-specification of Both Ground Pivots

5.1. Ab Initio Computation

The last problem under consideration is when both ground pivots are pre-specified. Consider fixing $A = A^* = 1$ and $B = B^* = 0$ so that the resulting variable list is $\mathbf{d} = \{l_{1s}, l_{2s}, l_{3s}, Q, Q^*\}$. Since we retain B, B^* at the origin like the pre-specification of one ground pivot formulation in Section 4, this system also has 41 moment parameters listed in 2. For this simplified system, the RML procedure computed all 503 solutions within 13 iterations and the path tracking success rate using double precision was 99%. Using only

a single processor, the total computation time was approximately three minutes. Figure 9 shows the ratio of number of repeats per iteration.

Since this system is small, it can be solved directly using standard homotopy continuation techniques without the use of RML in *Bertini*, a method not feasible for the other systems. This direct solve also resulted in 503 solutions from 7,362 tracked paths and took approximately ten minutes on a single processor. These 503 solutions are all distinct as the designs come in cognate groups of size one due to the pre-specified pivots.

5.2. Solution Set Validation

With such a small system that can be solved repeatedly and consistently reported 503 solutions, a statistical validation of the RML iterations was not necessary. Moreover, this solution count can be confirmed using the 2-homogeneous trace test summarized in Section 2.4. By switching the variable-parameter pair l_{1s} and g_{41} , the resulting system produced 129 solutions which can be directly computed with *Bertini*. The 2-homogeneous trace test was then successfully applied to a total of $503 + 129 = 632$ solutions confirming that 503 is indeed the precise solution count.

5.3. Applied Example

We consider the application of a wing folding mechanism as shown in Fig 11. The wing is made up of a planar 2R chain OCD with a proximal link OC and a distal link CD . The proximal link is connected to the fuselage using a rotary joint at O . Note that the 2R chain is by itself a two DoF system. For the folding this wing, three design configurations must be met, namely, a stowed configuration, an intermediate configuration, and a deployed configuration. The objective of this design challenge is to size a four-bar linkage (shown in black) with given ground pivot locations A and B , respectively, such that a chosen guide point X in the distal link of the 2R chain is guided approximately along the design positions, indicated in starred points, in a constrained manner.

We used the following specifications:

$$O = 0, A = 0.01 + 1.051i, A^* = 0.01 - 1.051i, \\ B = 0.137 - 0.211i, B^* = 0.137 + 0.211i, |OC| = 2.563, |CD| = 3.4, |CX| = 0.34.$$

The design positions to be met approximately are as listed in Appendix C. Note that the design positions specified are largely restricted to be within the reachable workspace of the guide-point X defined by the annular region as shown in Fig. 11. The desired curve is expected to intersect the workspace boundary in the stowed configuration and be tangential to it in the intermediate and deployed configurations.

Starting from 503 start points found during the *ab initio* run, a parameter homotopy run is carried out to the target system which represents the design problem of deployable wing mechanism. The successful

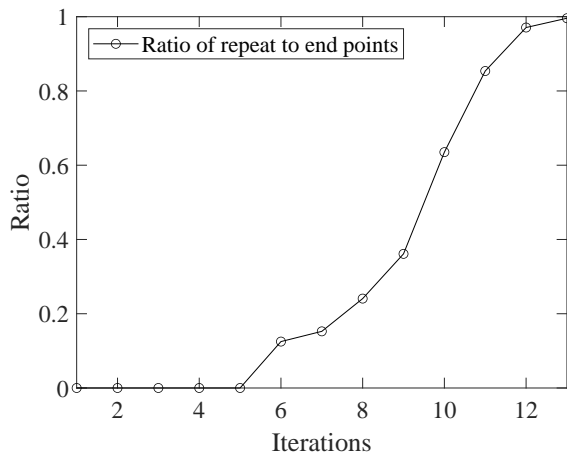


Figure 9: Ratio of repeat solutions per RML iteration when both ground pivots are pre-specified.

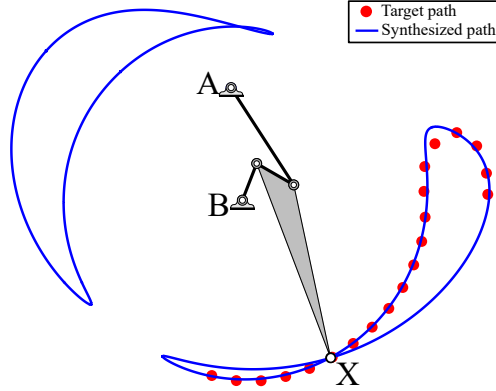


Figure 10: The chosen solution from which the final design was derived.

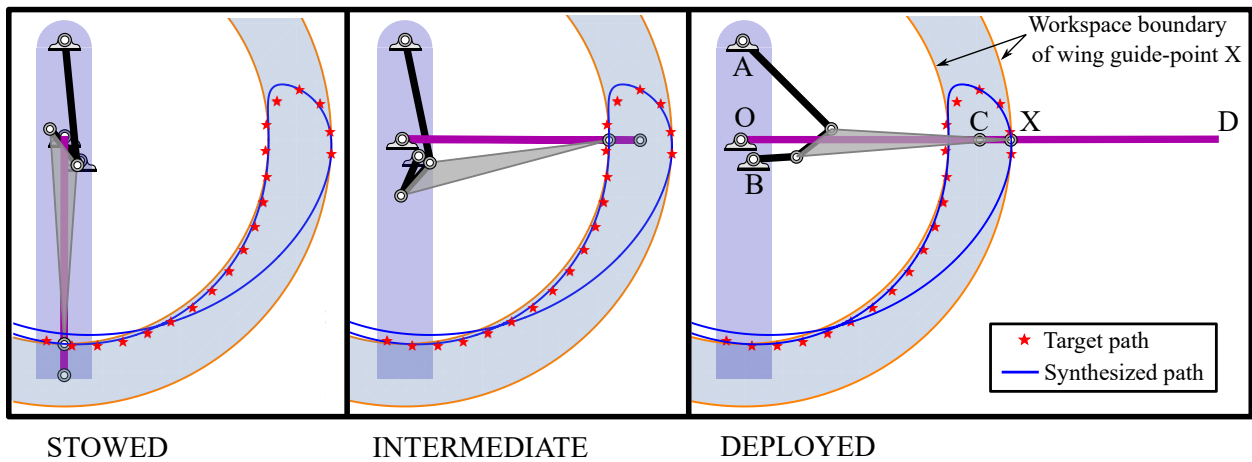


Figure 11: Three snapshots, namely, a stowed configuration, an intermediate configuration and a deployed configuration, of deployable aircraft wing mechanism.

paths yielded a subset of 27 physical solutions, of which 7 are local minima and 20 are saddle points. One of the local minima is found to be particularly effective in terms of packaging the system in the stowed configuration, which is shown in Fig. 11 at the three significant configurations of interest. For this plot, some minor corrections to the link dimensions of the overall system was made to ensure that the tangency conditions between the four-bar coupler curve and the workspace boundary of the wing guide-point X are met exactly at the intermediate and deployed configurations. The original solution computed from the parameter homotopy, before minor corrections, is presented in Fig. 10. This solution is the ninth-lowest cost, the dimensions are shown in Table D.11, with a cost value of 146.1838 and a maximum deviation of 0.7273.

6. Discussion

The approach used in this paper forms stationarity conditions for unconstrained kinematic optimization problems and deploys a root-finding algorithm that strives for completeness in finding the zeros (critical points) associated with these conditions. The concept of solving optimization problems this way is not new, but the contribution of this paper stems from the scale of the problems confronted. Specifically, this paper computes an unconstrained problem of $\approx 1,820,238$ roots, pushing the limits the authors' available compute power.

In this paper, we did not consider optimization constraints. Equality constraints were handled in the past with homotopy-based optimization [29], but we foresee the combinatorics associated with active/inactive inequality constraints posing a challenge in computational tractability. Solving the fully generic (no pivots specified) approximate four-bar path synthesis problem alongside several inequality constraints would not

be tractable with the computers used in this paper. Today’s current methods already easily incorporate inequality constraints using local [13, 22] or stochastic [9, 10] optimization techniques. Our approach is neither local (sensitive to initial guess) nor stochastic (non-deterministic), laying the groundwork for potentially more complete design space exploration. Inequality constraints conveniently enforce design requirements, such as ensuring that a pivot stays within a certain region or that a link stays less than a certain length. To incorporate inequality constraints using the methods of this paper, simplifying assumptions would need to be made, such as assuming the location of one (Section 4) or two (Section 5) ground pivots. This lack of inequality constraints does not prevent our solution set from admitting branch or circuit defective solutions. In the meanwhile, filtering the solutions after the computations adequately satisfies the requirements a designer may enforce on pivot locations and linkage lengths as well as remove the defective solutions.

This paper did not investigate the incorporation of inequality constraints. However, before such a challenge can be surmounted, the unconstrained problem needs to be investigated and characterized, which is the contribution of this paper. Our investigation discovered that the largest problem, the general case, required a large amount of computational resources, diminishing its practicality. Therefore, we included in our investigation two simplified cases (Sections 4 and 5) which trade-off generality for tractability, yielding more practical methods. Scaling up the methods of this paper to more complex multi-loop linkages, like a six-bar linkage, would not be tractable when considering the fully general (all dimensions unknown) synthesis problems. However, with the right pre-specifications, the unconstrained methods of this paper are extensible, e.g. consider converting the modular RR chain synthesis methods of [38] from exact to approximate. Furthermore, the coupler curve of any four-bar path generator can be translated anywhere in the plane by the inclusion of two more links [24, 23, 25], converting it into a six-bar. If this concession is made, the utility of inequality constraints discussed above diminishes.

7. Conclusions

Approximate kinematic synthesis is an appealing technique to find optimal designs of linkages. Previous optimization frameworks and solvers face the problem of settling on inferior local minima that may or may not depend on the initial solution guess and do not present a full set of the minima. Essentially, these methods fail to identify the landscape of the optimization problem. This paper presents a polynomial objective formulation to the approximate synthesis problem that can be solved via the polynomial homotopy continuation technique of random monodromy loops. The one-time solve for the critical points of this formulation, known as the *ab initio* solve, provides a starting solution set for which parameter homotopies can be applied to physically meaningful systems of interest. To produce a linearly parameterized system, we employed a first-moment formulation of the design parameters. The resulting system was solved for three cases: no pre-specifications on design dimensions (general case), a pre-specification on one ground pivot, and a pre-specification on both ground pivots. In each case, the resulting solutions sets were used as the basis from which we computed parameter homotopies to real design application examples. The resulting total generic solution set count for the general case, pre-specification of one ground pivot, and pre-specification of both ground pivots formulations are approximately $1,820,238 \pm 3810$, and exactly 26,052 and 503 points, respectively.

Acknowledgment

This material is based upon work supported by the National Science Foundation under Grant Nos. CMMI-2041789, CMMI-2144732, and CCF-2331400. We would like to thank Nicholas Deluca, Gabrielle Myers, and Katie Pala for construction of the gripper prototype. Finally, we thank Dr. Charles Wampler and the anonymous reviewers for their helpful comments.

Appendix A. Cognate Transformations for the General Case Formulation

For the four-bar represented in Fig. 2 with design variables $\mathbf{v}_1 = \{A, A^*, B, B^*, l_1, l_2, l_3, Q, Q^*\}$, the two other Roberts' cognates can be computed with the following cognate transformations:

$$\mathbf{v}_2 = \left\{ B, B^*, A + Q(B - A), A^* + Q^*(B^* - A^*), l_2\sqrt{(1-Q)(1-Q^*)}, \right. \\ \left. l_3\sqrt{(1-Q)(1-Q^*)}, l_1\sqrt{(1-Q)(1-Q^*)}, \frac{1}{1-Q}, \frac{1}{1-Q^*} \right\},$$

$$\mathbf{v}_3 = \left\{ A + Q(B - A), A^* + Q^*(B^* - A^*), A, A^*, l_3\sqrt{QQ^*}, l_1\sqrt{QQ^*}, \right. \\ \left. l_2\sqrt{QQ^*}, \frac{Q-1}{Q}, \frac{Q^*-1}{Q^*} \right\}.$$

Additionally, symmetric representation arising from relabeling of \mathbf{v}_1 is

$$\mathbf{v}'_1 = \{B, B^*, A, A^*, l_3, l_2, l_1, 1-Q, 1-Q^*\}.$$

The three Roberts' cognates and their symmetric representations yield $3 \cdot 2 = 6$ members to a group.

Appendix B. Cognate Transformations for the Pre-specification of One Ground Pivot

For the four-bar represented in Fig. 2 design variables $\mathbf{v}_1 = \{A, A^*, B, B^*, l_1, l_2, l_3, Q, Q^*\}$ such that $B = B^* = 0$, the Roberts' cognate that preserves the location of the fixed pivot can be computed as \mathbf{v}'_2 via Appendix A. Thus, there are 2 members to a group.

Appendix C. Design Positions and Parameters for the Applied Examples

The applied example for the general case used the continuous form of the moment parameters. The values used for the computation of the moments were derived from a recreation of the 6-bar kinematics and an interpolated and integration of the coupler curve. The resulting moments as described in Section 3 are given in Table C.5

$g_1 =$	-0.201259+0.571471 <i>i</i>	$g_{17} =$	-0.071325+0.12864 <i>i</i>	$g_{33} =$	-0.027377+0.043139 <i>i</i>
$g_2 =$	-0.250705-0.262911 <i>i</i>	$g_{18} =$	-0.051786-0.093304 <i>i</i>	$g_{34} =$	-0.016288-0.036071 <i>i</i>
$g_3 =$	0.223860-0.038956 <i>i</i>	$g_{19} =$	0.078593+0.006491 <i>i</i>	$g_{35} =$	-0.047476+0.101637 <i>i</i>
$g_4 =$	-0.0713+0.136836 <i>i</i>	$g_{20} =$	-0.037522+0.045931 <i>i</i>	$g_{36} =$	-0.05444-0.078008 <i>i</i>
$g_5 =$	-0.047476-0.101637 <i>i</i>	$g_{21} =$	0.223860+0.038956 <i>i</i>	$g_{37} =$	0.078593-0.006491 <i>i</i>
$g_6 =$	0.082306+0.016350 <i>i</i>	$g_{22} =$	-0.106001+0.154873 <i>i</i>	$g_{38} =$	-0.028084+0.057493 <i>i</i>
$g_7 =$	-0.201259-0.571471 <i>i</i>	$g_{23} =$	-0.071325-0.12864 <i>i</i>	$g_{39} =$	-0.027377-0.043139 <i>i</i>
$g_8 =$	0.416777+0.000000 <i>i</i>	$g_{24} =$	0.112046+0.000000 <i>i</i>	$g_{40} =$	0.040403+0.000000 <i>i</i>
$g_9 =$	-0.118802+0.25215 <i>i</i>	$g_{25} =$	-0.043775+0.07234 <i>i</i>	$g_{41} =$	-0.017369+0.026629 <i>i</i>
$g_{10} =$	-0.106001-0.154873 <i>i</i>	$g_{26} =$	-0.028084-0.057493 <i>i</i>	$g_{42} =$	0.082306-0.016350 <i>i</i>
$g_{11} =$	0.130889-0.001074 <i>i</i>	$g_{27} =$	0.048331+0.006554 <i>i</i>	$g_{43} =$	-0.023841+0.066922 <i>i</i>
$g_{12} =$	-0.05444+0.078008 <i>i</i>	$g_{28} =$	-0.0713-0.136836 <i>i</i>	$g_{44} =$	-0.037522-0.045931 <i>i</i>
$g_{13} =$	-0.023841-0.066922 <i>i</i>	$g_{29} =$	0.130889+0.001074 <i>i</i>	$g_{45} =$	0.048331-0.006554 <i>i</i>
$g_{14} =$	-0.250705+0.262911 <i>i</i>	$g_{30} =$	-0.051786+0.093304 <i>i</i>	$g_{46} =$	-0.016288+0.036071 <i>i</i>
$g_{15} =$	-0.118802-0.25215 <i>i</i>	$g_{31} =$	-0.043775-0.07234 <i>i</i>	$g_{47} =$	-0.017369-0.026629 <i>i</i>
$g_{16} =$	0.204155+0.000000 <i>i</i>	$g_{32} =$	0.065930+0.000000 <i>i</i>		

Table C.5: Numerical values of the 47 continuous moments of the general case applied example.

Tables C.6 and C.7 list the design positions for the applied examples in Section 4 and 5 with one ground pivot and both ground pivots pre-specified, respectively. In these tables, x is the real part and y is the imaginary part of the design positions. Note the points' respective complex conjugates are similar except for an opposite sign on the imaginary component.

#	x	y	#	x	y
1	0.364598	-1.05667	11	0.341038	-0.838013
2	0.365320	-1.03455	12	0.331590	-0.818017
3	0.365531	-1.01242	13	0.319373	-0.799592
4	0.365220	-0.990290	14	0.304292	-0.783430
5	0.364353	-0.968177	15	0.286853	-0.769836
6	0.362873	-0.946096	16	0.267863	-0.758491
7	0.360690	-0.924074	17	0.248001	-0.748736
8	0.357669	-0.902152	18	0.227699	-0.739930
9	0.353605	-0.880400	19	0.207204	-0.731578
10	0.348201	-0.858944	20	0.186667	-0.723333

Table C.6: Design positions of the applied example for the pre-specification of one ground pivot formulation.

#	x	y	#	x	y
1	-0.207019	-2.182090	11	2.063340	-0.938363
2	0.0687999	-2.239100	12	2.153400	-0.674308
3	0.347610	-2.240690	13	2.191820	-0.401537
4	0.624026	-2.193040	14	2.178680	-0.111425
5	0.892661	-2.102330	15	2.187730	0.167889
6	1.147710	-1.975820	16	2.302040	0.424395
7	1.383080	-1.821450	17	2.547380	0.549207
8	1.596310	-1.638030	18	2.771820	0.399482
9	1.783540	-1.427380	19	2.881780	0.093067
10	1.940770	-1.192140	20	2.896430	-0.145470

Table C.7: Design positions of the applied example for the pre-specification of both ground pivots formulation

Appendix D. Solution Values for the Applied Examples

The applied example solutions were evaluated by varied metrics. As the most optimal solution in cost may not always give the optimal design in terms of feasibility or aesthetics, it is important to consider other solutions, including saddle point solutions. The tables given in this section display the ten solutions with the lowest cost value. The real-value leg length variables are provided, one can employ the transformations given in Section 2.1 to compute the transformed variables. Additionally, maximum deviation between the design positions and solution path is provided as another metric to assess the solution goodness.

Appendix D.1. The General Case (No Dimensions Pre-specified)

The table D.8 gives the 10 solution values of the general case applied example based on lowest absolute cost value. Figure 5b, with Fig. 5a and Fig. 5d are among the lowest costs.

Figure D.12 shows the computed corresponding to the lowest absolute cost value. This solution is the global minimum, the other local minimum corresponds to the eighth solution of Table D.8. The other solutions in the table are saddle points. Cognate transformations for these solutions can be computed using the formulations given in Appendix A.

Appendix D.2. One Dimension Pre-specified

A challenge to choosing the solution with the lowest cost value in this situation is that the solution cognates are constrained to those only satisfying the dimension pre-specification. Usually, as in the general case, one may refer to a cognate solution from the group of six. However, in this scenario, we only have one other cognate that satisfies our dimension pre-specification.

Our computations recovered designs similar to the reference, [30], which was the inspiration for this example.

In fact, when sorting the solutions based off different error metrics, such as minimum nearest distance to the curve from a specified position, we can find designs such as this. This metric, as well as the max

	1	2	3	4	5
A	$-0.08538 - 0.04607i$	$-0.07627 - 0.06924i$	$-0.21686 - 0.3701i$	$-0.4184 + 0.04442i$	$-0.0406 - 0.3039i$
A^*	$-0.08538 + 0.04607i$	$-0.07627 + 0.06924i$	$-0.2168 + 0.3701i$	$-0.4184 - 0.04442i$	$-0.04056 + 0.3039i$
B	$-0.2767 - 0.8952i$	$-0.3427 - 0.1429i$	$0.08195 - 0.1943i$	$-0.09627 - 0.8621i$	$-0.2985 - 0.1947i$
B^*	$-0.2767 + 0.8952i$	$-0.3427 + 0.1429i$	$0.08195 + 0.1943i$	$-0.09627 + 0.8621i$	$-0.2985 + 0.1947i$
l_1	0.5907	0.1587	0.1102	0.6791	0.1897
l_2	0.4982	0.1815	0.1802	0.1415	0.1594
l_3	0.2158	0.06298	0.2866	0.4089	0.06938
Q	$0.1850 - 0.2617i$	$1.4693 + 2.7634i$	$-1.2155 - 1.1248i$	$0.3656 + 0.2638i$	$-0.6141 + 2.3195i$
Q^*	$0.1850 + 0.2617i$	$1.4693 - 2.7634i$	$-1.2155 + 1.1248i$	$0.3656 - 0.2638i$	$-0.6141 - 2.3195i$
Cost	$1.1568 \cdot 10^{-8}$	$1.7884 \cdot 10^{-8}$	$2.008746 \cdot 10^{-8}$	$3.6472 \cdot 10^{-8}$	$4.9846 \cdot 10^{-8}$
Max Dev	0.1676	0.09705	0.2075	0.4101	0.1149
	6	7	8	9	10
A	$-0.3992 + 0.006783i$	$-0.1787 - 0.5307i$	$-0.1420 - 0.9623i$	$-0.01113 - 0.2719i$	$-0.3533 + 0.03082i$
A^*	$-0.3992 - 0.006783i$	$-0.1787 + 0.5307i$	$-0.1420 + 0.9623i$	$-0.01113 + 0.2719i$	$-0.3533 - 0.03082i$
B	$-0.07725 - 0.2247i$	$-0.3854 - 0.7724i$	$-0.3883 - 0.1276i$	$-0.3620 - 0.1379i$	$-0.2093 - 0.06891i$
B^*	$-0.07725 + 0.2247i$	$-0.3854 + 0.7724i$	$-0.3883 + 0.1276i$	$-0.3620 + 0.1379i$	$-0.2093 + 0.06891i$
l_1	0.05930	0.1953	0.4462	0.2054	0.07326
l_2	0.2776	0.1412	0.1023	0.2222	0.1978
l_3	0.1761	0.3856	0.5249	0.05237	0.09384
Q	$1.9027 - 1.3375i$	$-1.1002 + 0.5747i$	$0.7603 - 0.3845i$	$-0.3771 + 1.8417i$	$1.9547 - 2.6906i$
Q^*	$1.9027 + 1.3375i$	$-1.1002 - 0.5747i$	$0.7603 + 0.3845i$	$-0.3771 - 1.8418i$	$1.9547 + 2.6906i$
Cost	$5.1537 \cdot 10^{-8}$	$6.134 \cdot 10^{-8}$	$6.7082 \cdot 10^{-8}$	$7.3460 \cdot 10^{-8}$	$1.6215 \cdot 10^{-7}$
Max Dev	0.1181	0.2304	0.4867	0.09704	0.1153

Table D.8: The dimensions of the top ten solutions as per lowest absolute cost value for the General Case example. Note that Fig. 5b, Fig. 5a, and Fig. 5d are the third, fifth, and ninth lowest costs, respectively.

	1	2	3	4	5
A	$0.1368 - 0.9734i$	$0.1345 - 0.9736i$	$0.1481 - 0.9355i$	$0.1696 - 0.9191i$	$0.1035 - 0.9839i$
A^*	$0.1368 + 0.9734i$	$0.1345 + 0.9736i$	$0.1481 + 0.9355i$	$0.1696 + 0.9191i$	$0.1035 + 0.9839i$
B	0	0	0	0	0
B^*	0	0	0	0	0
l_1	0.2385	0.2410	0.3127	0.3334	0.2710
l_2	0.1303	0.1392	0.6836	0.7303	0.2445
l_3	0.9854	0.9774	0.4179	0.3803	0.9945
Q	$-0.04980 + 0.05351i$	$-0.04520 + 0.05358i$	$-0.01631 + 0.1466i$	$-0.01317 + 0.1997i$	$0.006638 + 0.05778i$
Q^*	$-0.04980 - 0.05351i$	$-0.04520 - 0.05358i$	$-0.01631 - 0.1466i$	$-0.01317 - 0.1997i$	$0.006638 - 0.05778i$
Cost	0.1900	0.2004	0.2739	0.2846	0.4313
Max Dev	0.4474	0.4492	0.2951	0.2718	0.4426
	6	7	8	9	10
A	$0.3355 - 0.9478i$	$0.08979 - 0.9890i$	$0.3475 - 0.9477i$	$0.5021 - 1.1832i$	$0.006582 - 1.0334i$
A^*	$0.3355 + 0.9478i$	$0.08979 + 0.9890i$	$0.3475 + 0.9477i$	$0.5021 + 1.1832i$	$0.006582 + 1.033i$
B	0	0	0	0	0
B^*	0	0	0	0	0
l_1	0.1390	0.2858	0.1154	0.1845	0.2737
l_2	0.3832	0.2056	0.3245	2.1177	0.9582
l_3	1.2595	0.9595	1.2456	1.0345	0.1889
Q	$-0.2708 - 0.03743i$	$0.02692 + 0.04182i$	$-0.2573 - 0.09534i$	$0.1714 + 0.01781i$	$0.04203 - 0.1141i$
Q^*	$-0.2708 + 0.03743i$	$0.02692 - 0.04182i$	$-0.2573 + 0.09534i$	$0.1714 - 0.01781i$	$0.04203 + 0.11419i$
Cost	0.4477	0.4732	0.5072	0.5372	0.5447
Max Dev	0.09572	0.5198	0.1414	0.05264	0.2220

Table D.9: Table showing the dimensions of the ten lowest absolute costs values for the one dimension pre-specified applied example.

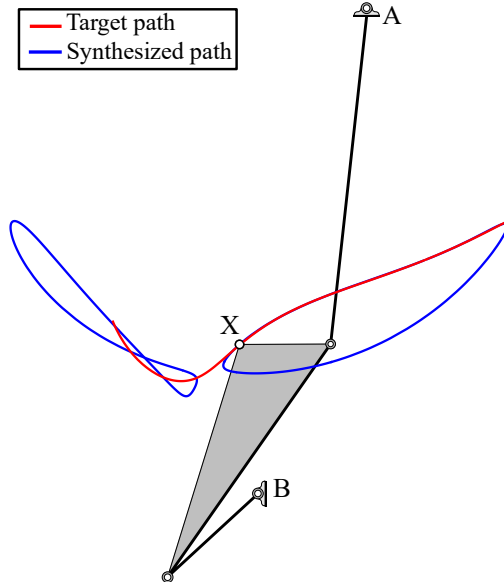


Figure D.12: The computed solution, the global minimum, with the absolute smallest cost function for the zero dimensions pre-specified example.

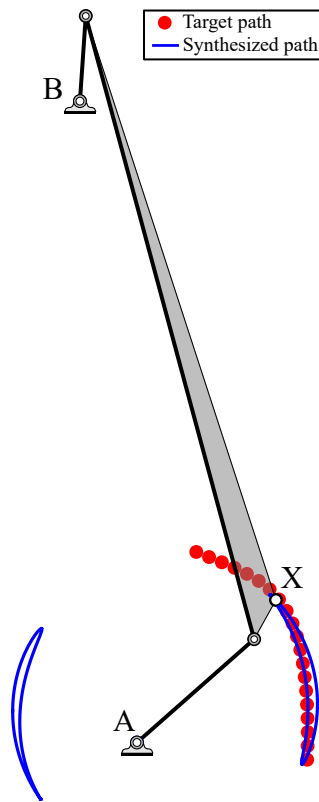


Figure D.13: The computed solution with the absolute smallest cost function for the one dimension pre-specified example.

distance between specified points and their nearest point on the solution curve (maximum deviation), is one such way to sort solutions. The design and design dimensions are presented in Fig. D.14. This solution is a saddle point and, although it bears a strong resemblance to the reference mechanism, it has too high a cost function for it to appear among desirable solutions when sorted by cost.

A	$-0.6836 + 0.3376i$
A^*	$-0.6836 - 0.3376i$
B	0
B^*	0
l_1	1.3570
l_2	0.1448
l_3	0.7440
Q	$0.4299 - 3.1614i$
Q^*	$0.4299 + 3.1614i$
Cost	2393.3919
Max Dev	0.4487

Table D.10: Numerical values of the one dimension pre-specified solution shown in Fig. D.14 that bears the highest resemblance to the reference path.

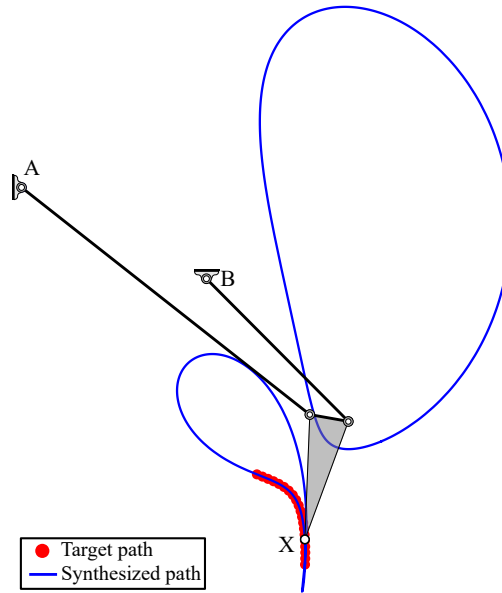


Figure D.14: The solution design, dimensions given in D.10, that bears the highest similarity to the reference design.

Appendix D.3. Two Dimensions Pre-specified

Since these values exhibit cognate groups of one member, these solution dimensions are the only designs available for the respective coupler curve.

References

- [1] Alt, H., 1923. Über die erzeugung gegebener ebener kurven mit hilfe des gelenkviereckes. *Z. Angew. Math. Mech.* 3, 13–19.
- [2] Baskar, A., Hills, C., Plecnik, M., Hauenstein, J.D., 2022. Estimating the Complete Solution Set of the Approximate Path Synthesis Problem for Four-Bar Linkages Using Random Monodromy Loops, in: *ASME 2022 International Design Engineering Technical Conferences and Computers and Information in Engineering Conference*, American Society of Mechanical Engineers Digital Collection.
- [3] Baskar, A., Plecnik, M., 2020. Synthesis of Six-bar Timed Curve Generators of Stephenson-type Using Random Monodromy Loops. *Journal of Mechanisms and Robotics* 13.
- [4] Baskar, A., Plecnik, M., 2021. Synthesis of Watt-Type Timed Curve Generators and Selection From Continuous Cognate Spaces. *Journal of Mechanisms and Robotics* 13.

	1	2	3	4	5
A	$0.01009 + 1.05063i$				
A^*	$0.01009 - 1.05063i$				
B	$0.13735 - 0.21073i$				
B^*	$0.13735 + 0.21073i$				
l_1	1.1469	1.1399	3.0964	1.2175	1.1043
l_2	1.2581	1.072	0.85531	0.90627	1.0913
l_3	1.1393	0.99409	2.3969	0.8673	0.97195
Q	$1.1173 + 1.2952i$	$0.4915 + 1.9561i$	$0.75885 + 0.35691i$	$-0.4148 + 2.2606i$	$0.8766 + 1.8144i$
Q^*	$1.1173 - 1.2952i$	$0.4915 - 1.9561i$	$0.75885 - 0.35691i$	$-0.4148 - 2.2606i$	$0.8766 - 1.8144i$
Cost	9.2773	16.4608	20.06176	20.19268	20.4224
Max Dev	1.6950	1.3245	2.4358	0.7240	1.6488

	6	7	8	9	10
A	$0.01009 + 1.05063i$				
A^*	$0.01009 - 1.05063i$				
B	$0.13735 - 0.21073i$				
B^*	$0.13735 + 0.21073i$				
l_1	1.1821	0.48908	0.67614	1.2972	1.2353
l_2	0.96274	1.0861	1.1545	0.48125	0.53218
l_3	0.91392	0.5814	0.72753	0.44298	0.49728
Q	$0.0235 + 2.2007i$	$2.1401 + 1.5928i$	$1.6628 + 1.6161i$	$-2.7666 + 3.0684i$	$-1.6424 + 3.5032i$
Q^*	$0.0235 - 2.2007i$	$2.1401 - 1.5928i$	$1.6628 - 1.6161i$	$-2.7666 - 3.0684i$	$-1.6424 - 3.5032i$
Cost	28.6785	52.2681	76.2607	146.1838	167.1347
Max Dev	0.9492	0.7084	1.04291	0.7273	0.70473

Table D.11: Table showing the dimensions of the ten lowest absolute costs values for the two dimension pre-specified applied example.

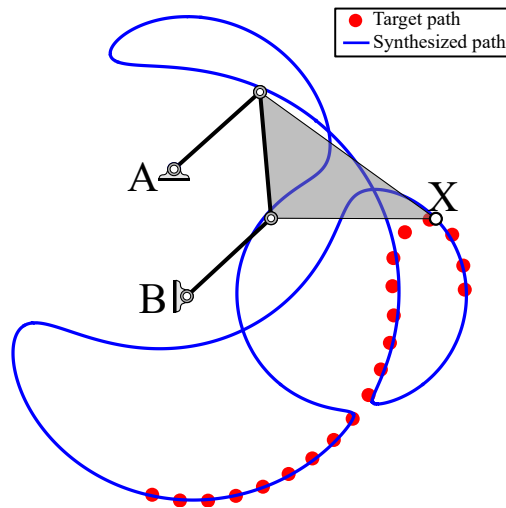


Figure D.15: The computed solution with the absolute smallest cost function for the two dimension pre-specified example.

- [5] Bates, D.J., Hauenstein, J.D., Sommese, A.J., Wampler, C.W., . Bertini: Software for Numerical Algebraic Geometry.
- [6] Bates, D.J., Hauenstein, J.D., Sommese, A.J., Wampler, C.W., 2013. Numerically Solving Polynomial Systems with Bertini. SIAM.
- [7] Blechschmidt, J.L., Uicker, Jr., J.J., 1986. Linkage Synthesis Using Algebraic Curves. Journal of Mechanisms, Transmissions, and Automation in Design 108, 543–548.
- [8] Brake, D.A., Hauenstein, J.D., Liddell, A.C., 2016. Decomposing Solution Sets of Polynomial Systems Using Derivatives, in: Greuel, G.M., Koch, T., Paule, P., Sommese, A. (Eds.), Mathematical Software – ICMS 2016, Springer International Publishing, Cham. pp. 127–135.

- [9] Bulatović, R.R., Miodragović, G., Bošković, M.S., 2016. Modified Krill Herd (MKH) algorithm and its application in dimensional synthesis of a four-bar linkage. *Mechanism and Machine Theory* 95, 1–21.
- [10] Bulatović, R.R., Đorđević, S.R., Đorđević, V.S., 2013. Cuckoo Search algorithm: A metaheuristic approach to solving the problem of optimum synthesis of a six-bar double dwell linkage. *Mechanism and Machine Theory* 61, 1–13.
- [11] Duff, T., Hill, C., Jensen, A., Lee, K., Leykin, A., Sommars, J., 2019. Solving polynomial systems via homotopy continuation and monodromy. *IMA Journal of Numerical Analysis* 39, 1421–1446.
- [12] Ebrahimi, S., Payvandy, P., 2015. Efficient constrained synthesis of path generating four-bar mechanisms based on the heuristic optimization algorithms. *Mechanism and Machine Theory* 85, 189–204.
- [13] Fox, R.L., Willmert, K.D., 1967. Optimum Design of Curve-Generating Linkages With Inequality Constraints. *Journal of Engineering for Industry* 89, 144–151.
- [14] Guigue, A., Hayes, M., 2016. Continuous approximate synthesis of planar function-generators minimising the design error. *Mechanism and Machine Theory* 101, 158–167. doi:10.1016/j.mechmachtheory.2016.03.012.
- [15] Guo, L., Zhang, Y., Wu, J., an Yao, Y., 2023. Combination of different trajectory description approaches improves the trajectory synthesis performance: Validation by a coarse-to-fine method. *Mechanism and Machine Theory* 187, 105370. URL: <https://www.sciencedirect.com/science/article/pii/S0094114X23001416>, doi:<https://doi.org/10.1016/j.mechmachtheory.2023.105370>.
- [16] Hauenstein, J.D., Oeding, L., Ottaviani, G., Sommese, A.J., 2019. Homotopy techniques for tensor decomposition and perfect identifiability. *Journal für die reine und angewandte Mathematik (Crelles Journal)* 2019, 1–22.
- [17] Hauenstein, J.D., Rodriguez, J.I., 2020. Multiprojective witness sets and a trace test. *Advances in Geometry* 20, 297–318.
- [18] Hauenstein, J.D., Sherman, S.N., 2022. Using Monodromy to Statistically Estimate the Number of Solutions, in: Holderbaum, W., Selig, J.M. (Eds.), 2nd IMA Conference on Mathematics of Robotics, Springer International Publishing, Cham. pp. 37–46.
- [19] Hauenstein, J.D., Sommese, A.J., 2010. Witness sets of projections. *Applied Mathematics and Computation* 217, 3349–3354.
- [20] Koladiya, D., Shiakolas, P.S., Kebrle, J., 2008. Evolutionary Based Optimal Synthesis of Four-Bar Mechanisms, in: ASME 2003 International Mechanical Engineering Congress and Exposition, American Society of Mechanical Engineers Digital Collection. pp. 539–544.
- [21] Kramer, S.N., Sandor, G.N., 1975. Selective Precision Synthesis—A General Method of Optimization for Planar Mechanisms. *Journal of Engineering for Industry* 97, 689–701.
- [22] Lewis, D.W., Gyory, C.K., 1967. Kinematic Synthesis of Plane Curves. *Journal of Engineering for Industry* 89, 173–175.
- [23] Lusk, C., 2022a. Forty-two Watt I indirect cognates of a four-bar via angular-velocity graph coloring, in: ASME 2022 International Design Engineering Technical Conferences and Computers and Information in Engineering Conference, American Society of Mechanical Engineers Digital Collection.
- [24] Lusk, C., 2022b. Watt I indirect cognates of four-bar linkages, in: USCToMM Symposium on Mechanical Systems and Robotics, Springer International Publishing. pp. 90–99.
- [25] Lusk, C., 2023. Exact placement of ground pivots using Watt I indirect cognates of a four-bar mechanism, in: ASME 2023 International Design Engineering Technical Conferences and Computers and Information in Engineering Conference, American Society of Mechanical Engineers Digital Collection.

- [26] McDougall, R., Nokleby, S., 2009. Synthesis of Grashof Four-Bar Mechanisms Using Particle Swarm Optimization, in: ASME 2008 International Design Engineering Technical Conferences and Computers and Information in Engineering Conference, American Society of Mechanical Engineers Digital Collection. pp. 1471–1475.
- [27] Morgan, A.P., Sommese, A.J., 1989. Coefficient-parameter polynomial continuation. *Applied Mathematics and Computation* 29, 123–160.
- [28] Morgan, A.P., Wampler, II, C.W., 1990. Solving a Planar Four-Bar Design Problem Using Continuation. *Journal of Mechanical Design* 112, 544–550.
- [29] O'Connor, S., Plecnik, M., Baskar, A., Joo, J., 2023. Complete solutions for the approximate synthesis of spherical four-bar function generators, in: ASME 2023 International Design Engineering Technical Conferences and Computers and Information in Engineering Conference, American Society of Mechanical Engineers Digital Collection.
- [30] Plecnik, M.M., Fearing, R.S., 2017. A Study on Finding Finite Roots for Kinematic Synthesis, in: ASME 2017 International Design Engineering Technical Conferences and Computers and Information in Engineering Conference, American Society of Mechanical Engineers. pp. V05BT08A083–V05BT08A083.
- [31] Rao, R., Pawar, R., 2020. Constrained design optimization of selected mechanical system components using rao algorithms. *Applied Soft Computing* 89, 106141. URL: <https://www.sciencedirect.com/science/article/pii/S1568494620300818>, doi:<https://doi.org/10.1016/j.asoc.2020.106141>.
- [32] Roberts, S., 1875. On Three-bar Motion in Plane Apace. *Proceedings of the London Mathematical Society* 1, 14–23.
- [33] Sarkisyan, Y.L., Gupta, K.C., Roth, B., 1973. Kinematic Geometry Associated With the Least-Square Approximation of a Given Motion. *Journal of Engineering for Industry* 95, 503–510.
- [34] Selvi, Ö., Yavuz, S., 2018. Design and Dimensional Optimization of a Novel Walking Mechanism with Firefly Algorithm, in: Dede, M.I.C., Itik, M., Lovasz, E.C., Kiper, G. (Eds.), *Mechanisms, Transmissions and Applications*, Springer International Publishing, Cham. pp. 67–75.
- [35] Shin, W.D., Stewart, W., Estrada, M.A., Ijspeert, A.J., Floreano, D., 2023. Elastic-actuation mechanism for repetitive hopping based on power modulation and cyclic trajectory generation. *IEEE Transactions on Robotics* 39, 558–571.
- [36] Slesongsom, S., Bureerat, S., 2018. Optimal Synthesis of Four-Bar Linkage Path Generation through Evolutionary Computation with a Novel Constraint Handling Technique. *Computational Intelligence and Neuroscience* 2018, e5462563.
- [37] Smaili, A., Diab, N., 2007. Optimum synthesis of hybrid-task mechanisms using ant-gradient search method. *Mechanism and Machine Theory* 42, 115–130.
- [38] Soh, G.S., McCarthy, J.M., 2008. The synthesis of six-bar linkages as constrained planar 3R chains. *Mechanism and Machine Theory* 43, 160–170. doi:10.1016/j.mechmachtheory.2007.02.004.
- [39] Sommese, A.J., Wampler, C.W., 2005. *The Numerical Solution of Systems of Polynomials Arising in Engineering and Science*. World Scientific, Singapore.
- [40] Subbian, T., Flugrad, Jr., D.R., 1991. Four-Bar Path Generation Synthesis by a Continuation Method. *Journal of Mechanical Design* 113, 63–69.
- [41] Tsai, L.W., Lu, J.J., 1990. Coupler-Point-Curve Synthesis Using Homotopy Methods. *Journal of Mechanical Design* 112, 384–389.
- [42] Wampler, C.W., 1996. Isotropic coordinates, circularity, and Bézout numbers: Planar kinematics from a new perspective, in: *Proceedings of the ASME 1996 IDETC/CIE Conference*, Irvine, California.
- [43] Wampler, C.W., Morgan, A.P., Sommese, A.J., 1992. Complete Solution of the Nine-Point Path Synthesis Problem for Four-Bar Linkages. *Journal of Mechanical Design* 114, 153–159.